

Erratum: Systematic study of (γ, n) reaction rates for $Z \geq 78$ isotopes [Phys. Rev. C **70**, 035802 (2004)]

K. Sonnabend, K. Vogt, D. Galaviz, S. Müller, and A. Zilges*
*Institut für Kernphysik, Technische Universität Darmstadt,
Schlossgartenstr. 9, D-64289 Darmstadt, Germany*
(Dated: November 10, 2018)

A typographical error occurred in Table I of the original paper [1]. The natural abundance of ^{196}Hg was cited incorrectly. The correct value is $(0.15 \pm 0.01)\%$.

The unit of the photon flux N_γ plotted as the ordinate in Figure 2 of the original paper [1] is incomplete. The unit should read $\text{keV}^{-1}\text{cm}^{-2}\text{s}^{-1}$.

The half-lives of the Hg isotopes have been remeasured by [2]. These values were used in the analysis if their accuracy was significantly improved compared to the values given in [3]. Thus, column four of Table II of the original paper [1] has been corrected (see Table I).

During the preparation of this erratum the error propagation was checked, too. The approximation of the Planck distribution is possible with an overall mean deviation of about 5 - 10%. This uncertainty has been included in the statistical errors presented in Table VII of the original paper [1]. However, we found that a systematical uncertainty of about 20% was mentioned in the text in the special case of ^{204}Hg but it was not included in the results presented in Table VII of the original paper [1]. This systematic uncertainty results from an un-

*Electronic address: zilges@ikp.tu-darmstadt.de

derestimation of the photon flux, thus, the reaction rate is underestimated, too. The corrected reaction rate is $\lambda_{\text{exp}}^{\text{super}}(^{204}\text{Hg}) = (57 \pm 9 + 12) \text{ s}^{-1}$.

Furthermore, the results of the ground-state reaction rates for the Pt isotopes have changed compared to previous publications [4, 5] due to an improved analysis. The differences are described in detail in [6].

The final results for the ground-state reaction rates presented in [1] are not influenced by these corrections.

Finally, we want to stress that the neutron density during r -process nucleosynthesis is well above 10^{20} cm^{-3} (see e.g. [7]).

Acknowledgments

We thank P. Mohr for his careful reading of the original paper. This work was supported by the Deutsche Forschungsgemeinschaft under contract SFB 634.

-
- [1] K. Sonnabend, K. Vogt, D. Galaviz, S. Müller, and A. Zilges, Phys. Rev. C **70**, 035802 (2004).
[2] K. Lindenberg, F. Neumann, D. Galaviz, T. Hartmann, P. Mohr, K. Vogt, S. Volz, and A. Zilges, Phys. Rev. C **63**, 047307 (2001).
[3] ENSDF, NNDC Online Data Service, ENSDF database, <http://www.nndc.bnl.gov/nndc/ensdf/> (2003).
[4] P. Mohr, K. Vogt, M. Babilon, J. Enders, T. Hartmann, C. Hutter, T. Rauscher, S. Volz, and A. Zilges, Phys. Lett. B **488**, 127 (2000).
[5] K. Vogt, P. Mohr, M. Babilon, J. Enders, T. Hartmann, C. Hutter, T. Rauscher, S. Volz, and A. Zilges, Phys. Rev. C **63**, 055802 (2001).
[6] K. Vogt, Ph.D. thesis, Institut für Kernphysik, TU Darmstadt (2003).
[7] K.-L. Kratz, J.-P. Bitouzet, F.-K. Thielemann, P. Möller, and B. Pfeiffer, Astrophys. J. **403**, 216 (1993).

TABLE I: Properties of the reactions $^{196,198,204}\text{Hg}(\gamma,n)$ and the following decays of the produced unstable isotopes $^{195,197,203}\text{Hg}$. Additionally, the reactions $^{198}\text{Hg}(\gamma,n)^{197m}\text{Hg}(\gamma)$ and $^{199}\text{Hg}(\gamma,\gamma')^{199m}\text{Hg}(\gamma)$ are listed. Half-lives of $^{195,197,199m}\text{Hg}$ were taken from [2], other data was taken from [3].

Seed	S_n / keV	Product	Decay: $T_{1/2}$	E_γ / keV	I_γ / %
^{196}Hg	8839 ± 50	^{195}Hg	$\epsilon: (10.53 \pm 0.03) \text{ h}$	61.46 ± 0.03	6.19 ± 0.76
				779.80 ± 0.05	6.8 ± 0.7
				1111.04 ± 0.10	1.44 ± 0.20
^{198}Hg	8484 ± 3	^{197}Hg	$\epsilon: (64.94 \pm 0.07) \text{ h}$	77.351 ± 0.002	18.7 ± 0.4
				191.36 ± 0.02	0.63 ± 0.02
				268.71 ± 0.03	0.039 ± 0.002
^{204}Hg	7495 ± 2	^{203}Hg	$\beta^-: (46.61 \pm 0.02) \text{ d}$	279.197 ± 0.001	81.46 ± 0.13
^{198}Hg	≈ 8962	^{197m}Hg	$\gamma: (23.8 \pm 0.1) \text{ h}$	133.08 ± 0.05	33.48 ± 0.26
^{199}Hg	—	^{199m}Hg	$\gamma: (42.67 \pm 0.09) \text{ min}$	158.3 ± 0.1	52.3 ± 1.0
				374.1 ± 0.1	13.8 ± 1.1

Systematic study of (γ, n) reaction rates for $Z \geq 78$ isotopes

K. Sonnabend, K. Vogt, D. Galaviz, S. Müller, and A. Zilges*

Institut für Kernphysik, Technische Universität Darmstadt,

Schlossgartenstr. 9, D-64289 Darmstadt, Germany

(Dated: November 10, 2018)

Abstract

The (γ, n) reaction rates of the isotopes $^{196,198,204}\text{Hg}$ and ^{204}Pb have been determined using the photoactivation technique in an energy region relevant for p process nucleosynthesis. The systematic study of the ground-state (γ, n) reaction rates on even-even nuclei in the mass region $Z \geq 78$ is complemented with these experiments. The data are compared to rates predicted in the framework of two statistical model approaches.

PACS numbers: 25.20.-x, 26.30.+k, 27.80.+w

arXiv:astro-ph/0409040v2 6 Jan 2005

*Electronic address: zilges@ikp.tu-darmstadt.de

I. INTRODUCTION

The heavy nuclei with $Z \geq 26$ are mainly produced by the astrophysical s and r process. Both describe nucleosynthesis by neutron capture reactions with subsequent β decays. The s process takes place during quiescent burning phases of medium mass stars (mean neutron density $n_n \approx 2 - 4 \times 10^8 \text{ cm}^{-3}$, mean temperature $kT \approx 25 \text{ keV}$ [1]). In contrast, the r process requires explosive environments ($n_n \approx 10^{20} \text{ cm}^{-3}$, $T \approx 3 \times 10^9 \text{ K}$ [2]).

However, 35 stable isotopes on the proton rich side of the valley of stability cannot be produced by either of these processes. A complete list of the so-called p nuclei can be found in [3, 9]. Their natural abundances are in the order of 0.01% to 1%, a hint for their production in a secondary process. The only exceptions from the low abundances are $^{92,94}\text{Mo}$ and ^{96}Ru . One has to distinguish between the p process in the mass region $Z \leq 50$ (e.g. rp process [4, 5]) and at higher masses where photodisintegration reactions like (γ, n) , (γ, α) , and (γ, p) play the important role.

The latter reactions take place at temperatures of $T = 2 - 3 \times 10^9 \text{ K}$ and the whole process lasts in the order of seconds. Possible astrophysical sites for this process are the oxygen- and neon-rich layers of type II supernovae. However, a definite conclusion is still missing. Details of the reaction path sometimes denoted as γ process can be found in various reviews [2, 3, 6, 7, 8, 9].

The reaction network of the p process is very extensive dealing with around 2000 nuclei and several thousand corresponding reaction rates. Thus, it is mandatory to use theoretical predictions because many of the nuclei involved are not accessible with the present experimental methods. However, it was recently emphasized by Arnould and Goriely [9] that the present lack of measured reaction rates in the astrophysically relevant energy region is a constraint on the reliability of theoretical predictions. Most of the existing experimental data on photodisintegration rates was measured around the Giant Dipole Resonance, therefore, being far off the energy region of interest for p process nucleosynthesis lying close above the reaction threshold.

The (γ, n) reaction rates of the most proton rich stable isotopes can be measured by photoactivation. High resolution γ spectroscopy of transitions in the daughter nuclei of the produced unstable isotopes allows a very high sensitivity. However, the experiments are sometimes hampered by high neutron separation energies S_n and very low abundances of

the isotopes of interest.

In this manuscript we present the results of a systematic investigation of even-even neutron rich isotopes with $Z \geq 78$. The experimental method is presented in Section II followed by a description of two different ways to evaluate the data. Section IV summarizes the results for the observed Hg and Pb isotopes. A comparison to different theoretical predictions is drawn in Section V including previous results on $^{190,192,198}\text{Pt}$ and ^{197}Au . We conclude with a summary and outlook.

II. EXPERIMENTAL METHOD

The experiments were performed at the superconducting Darmstadt electron accelerator S-DALINAC [10]. The monoenergetic electron beam is fully stopped in a thick copper radiator target. Thus, a continuous bremsstrahlung spectrum is produced with energies up to the electron energy E_{max} . The targets are usually placed behind a collimator made of copper to get a well defined beam spot. The absolute intensity of the photon beam is determined by an online measurement of the reaction $^{11}\text{B}(\gamma,\gamma')$ using two high-purity germanium detectors. The energy distribution results from a Monte Carlo simulation that is fitted to these data at several energies E_{max} . Details of the setup are described in [11, 12, 13].

If a higher photon intensity is needed, e.g. due to a low amount of target material, the targets are positioned directly behind the radiator target where the intensity of the beam is about a factor of 300 higher. Here the determination of the absolute photon intensity is realized by measuring relative to a standard reaction. Either the reaction $^{197}\text{Au}(\gamma,\text{n})$ or $^{187}\text{Re}(\gamma,\text{n})$ is used. The cross sections of both reactions are well known close above their respective reaction thresholds [14, 15].

The targets are typically irradiated between 12 and 24 hours depending on the expected activation rate. Afterwards, the yield of the produced unstable isotopes is measured offline. For this purpose the γ rays emitted after the β decay of the unstable nuclei are detected.

The targets are mounted in front of a well shielded HPGe detector. The number of γ rays Y is directly proportional to the integrated product of the (γ,n) cross section $\sigma(E)$ and the photon flux $N_\gamma(E, E_{\text{max}})$, i.e.:

$$Y \propto \int_0^\infty N_\gamma(E, E_{\text{max}})\sigma(E)dE \quad (1)$$

TABLE I: Properties of the targets and calibration standards used for the photoactivation experiments.

target	masses	obs. isotopes	nat. abundances [16]
$^{\text{nat}}\text{Pb}$	435 – 443 mg	^{204}Pb	$(1.4 \pm 0.1)\%$
		^{196}Hg	$(0.15 \pm 0.01)\%$
$^{\text{nat}}\text{HgS}$	1.97 – 2.72 g	^{198}Hg	$(9.97 \pm 0.08)\%$
		^{204}Hg	$(6.87 \pm 0.04)\%$
$^{\text{nat}}\text{B}$	636 – 846 mg	^{11}B	$(80.1 \pm 0.2)\%$
$^{\text{nat}}\text{Au}$	151 – 165 mg	^{197}Au	100%

The factor of proportionality depends on the activation time as well as on the absolute detector efficiency and the absolute intensity of the observed γ decay line. For a detailed discussion see Ref. [13].

Due to the high sensitivity of the photoactivation technique one can use naturally composed target material in many cases. Metallic discs were used for the investigation of Pb whereas for the observation of the Hg isotopes the targets were composed of HgS powder that was pressed into thin tablets. The properties of the targets as well as of the calibration standards used are listed in Table I.

The Pb targets were activated behind the collimator using ^{11}B as well as ^{197}Au to determine the photon beam intensity. Thus, a disc of Au and one of Pb were sandwiched between two thin layers of boron. Due to the low abundance of ^{196}Hg , the Hg targets were placed in the more intense photon flux directly behind the radiator target. They were mounted between two thin foils of Au to calibrate the photon beam intensity.

III. DATA ANALYSIS

The (γ, n) reaction rate $\lambda(T)$ for a nucleus in a thermal photon bath at a certain temperature T is given by

$$\lambda(T) = \int_0^\infty cn_\gamma(E, T)\sigma(E)dE \quad (2)$$

where c is the speed of light and $\sigma(E)$ is the cross section of the (γ, n) reaction. The number of photons with energy E per unit volume and energy interval $n_\gamma(E, T)$ is described by the

Planck distribution

$$n_\gamma(E, T) = \left(\frac{1}{\pi}\right)^2 \left(\frac{1}{\hbar c}\right)^3 \frac{E^2}{\exp(E/kT) - 1} \quad (3)$$

In order to determine the reaction rate $\lambda(T)$ at a given temperature T Eq. 2 offers two possibilities: one can either derive the energy dependence of the cross section $\sigma(E)$ and calculate $\lambda(T)$ using Eqs. 2 and 3 or measure the reaction rate $\lambda(T)$ directly by approximating the Planck distribution of photons at a given temperature in the astrophysically relevant energy range. The former case is the *conventional* method whereas the latter one will be called the *superposition* method. The pros and cons of the two methods are explained in the following paragraphs.

A. The superposition method

It is very useful to derive the experimental reaction rates without any assumption about the shape of the cross section close to the threshold. Therefore, the superposition method approximates the Planck distribution of Eq. 3 by a superposition of several bremsstrahlung spectra with different endpoint energies in the region of astrophysical interest.

Figure 1 shows the Planck distribution at $T = 2.5 \times 10^9$ K, a typical (γ, n) cross section and the product of both at this temperature (see Eq. 2). It is obvious that an approximation of the Planck distribution in a rather narrow Gamow-like energy window above the threshold energy is sufficient to derive the reaction rate $\lambda(T)$ without further assumptions.

Figure 2 shows the approximation for $T = 2.5 \times 10^9$ K using six bremsstrahlung spectra with $E_{\max} \in [8325, 9900]$ keV. Depending on the temperature T the bremsstrahlung spectra $N_\gamma(E, E_{\max, i})$ have to be weighted by factors $a_i(T)$:

$$cn_\gamma(E, T) \approx \sum_i a_i(T) N_\gamma(E, E_{\max, i}) \quad (4)$$

Combining Eqs. 1 and 4 with the definition of the ground-state reaction rate $\lambda(T)$ (see Eq. 2) one gets a fully model independent expression:

$$\begin{aligned} \lambda(T) &\approx \sum_i a_i(T) \int N_\gamma(E, E_{\max, i}) \sigma(E) dE \\ &\propto \sum_i a_i(T) Y_i \end{aligned} \quad (5)$$

Note that it is possible to choose the temperature T off-line by simply adjusting the weighting factors $a_i(T)$ once the yields Y_i have been determined from the experimental data. It

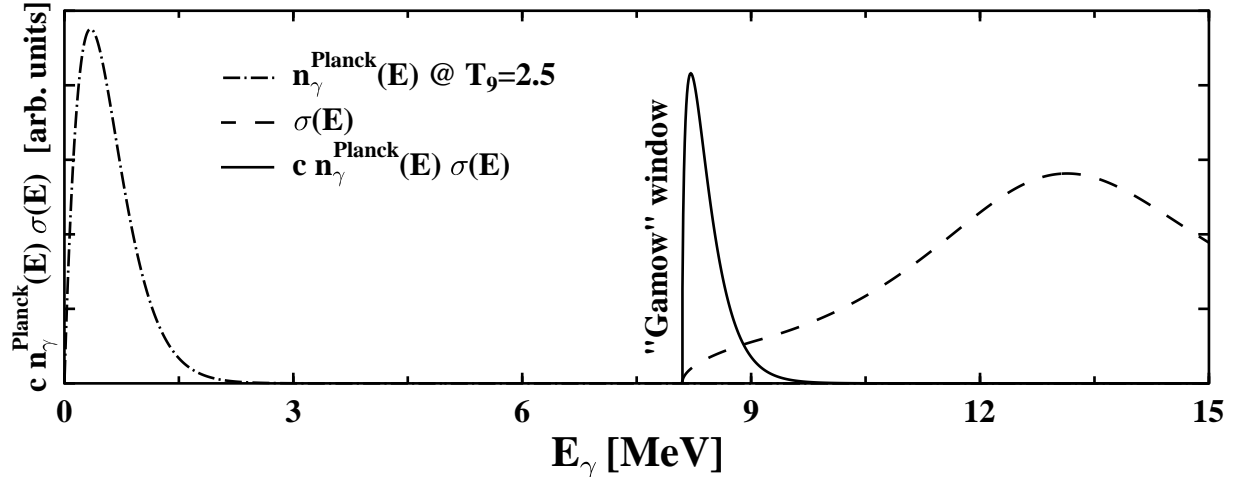


FIG. 1: The Gamow-like energy window for (γ, n) reactions. The Planck distribution corresponding to a temperature $T = 2.5 \times 10^9$ K is drawn (dashed-dotted line). Note that this distribution shows an exponential decrease. A (γ, n) cross section with the Giant Dipole Resonance around 13 MeV and a typical threshold behavior is plotted (dashed line). The product of both curves – the integrand of Eq. 2 – yields a Gamow-like energy window as known from charged particle reactions above the neutron separation energy S_n .

is sufficient to measure at five to seven different energies E_{\max} to get a good approximation with deviation of less than about 10% of the Planck distribution in the astrophysically relevant energy region and for temperatures in the range from $T = 2.0 - 3.0 \times 10^9$ K.

The superposition method uses the high intensities of photon fluxes that are available if bremsstrahlung spectra are taken for the activation of the targets. Thus, it has been possible to determine experimentally the ground-state reaction rates of rare proton rich isotopes like ^{196}Hg . points of the p process reaction network. In addition the influence of resonances in the Gamow-like energy window is included because of the continuous character of the photon energy distribution.

B. The conventional method

The setup we have used for the activation experiments is limited to an energy of $E_{\max} = 10$ MeV. Depending on the investigated nucleus it is not always possible to use the superposition method with reasonable accuracy. In these cases we have applied the con-

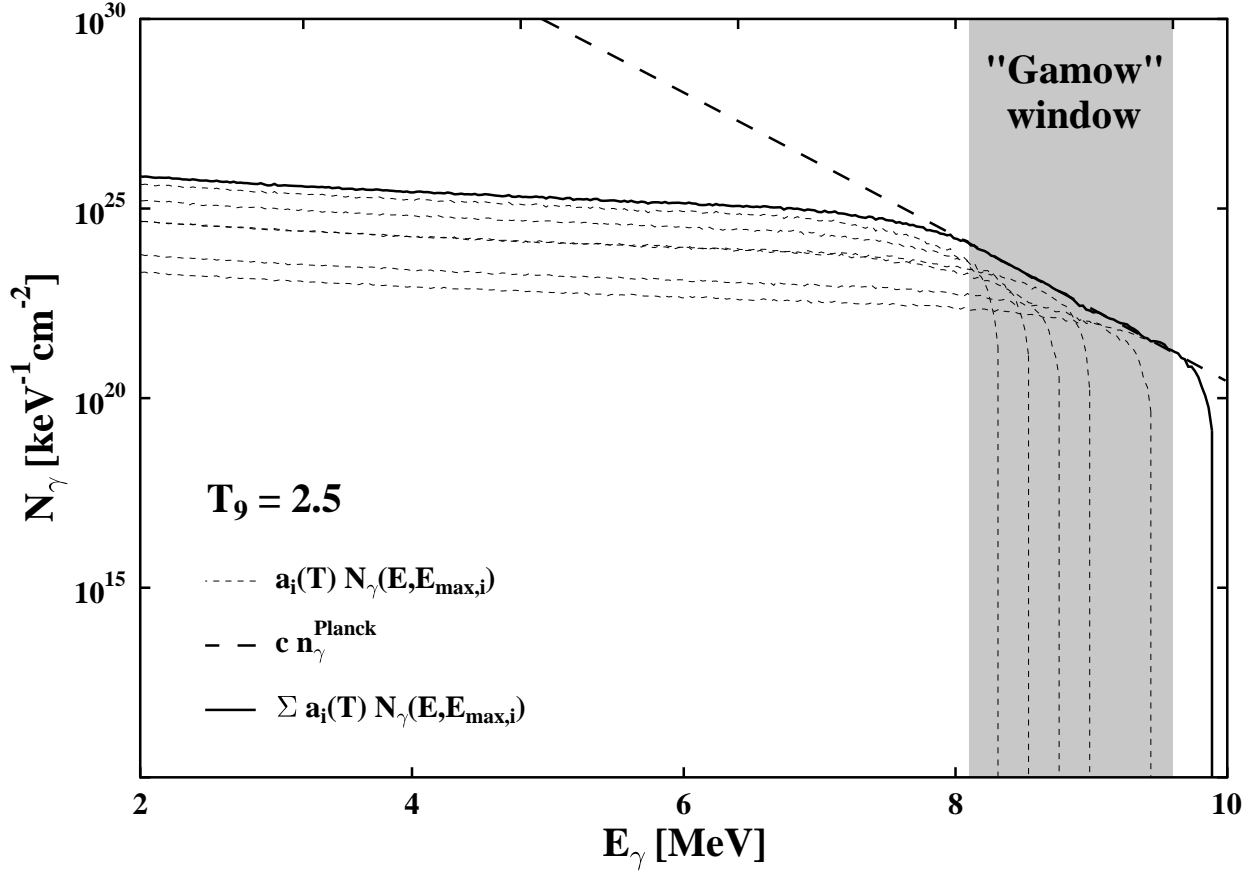


FIG. 2: Approximation of the Planck distribution by bremsstrahlung spectra. The grey shaded area corresponds to the Gamow-like energy window i.e. the relevant energy region for p process nucleosynthesis. The six bremsstrahlung spectra are weighted by temperature dependent factors $a_i(T)$ (thin dashed lines). They are summed (solid line) to approximate the Planck distribution (dashed line).

ventional method. Here we have to assume a certain energy dependence of the (γ, n) cross section near threshold.

$$\sigma(E) = \sigma_0 \left(\frac{E - S_n}{S_n} \right)^{0.5} \quad (6)$$

S_n is the threshold of the (γ, n) reaction, the exponent $k = 0.5$ corresponds to a pure s wave neutron emission. The normalization factor σ_0 can be derived from the experimental activation data to calculate the reaction rate using Eq. 2.

Obviously, this method depends strongly on the correctness of the assumed threshold behavior. However, a direct measurement of the energy dependence, e.g. with monoenergetic photons as described in [17], is often difficult due to the large amounts of isotopically enriched

TABLE II: Properties of the reactions $^{196,198,204}\text{Hg}(\gamma, n)$ and the following decays of the produced unstable isotopes $^{195,197,203}\text{Hg}$. Additionally, the reactions $^{198}\text{Hg}(\gamma, n)^{197m}\text{Hg}(\gamma)$ and $^{199}\text{Hg}(\gamma, \gamma')^{199m}\text{Hg}(\gamma)$ are listed. Data taken from [18].

seed	S_n / keV	product	decay: $T_{1/2}$	E_γ / keV	I_γ / %
^{196}Hg	8839 ± 50	^{195}Hg	ϵ : (9.9 ± 0.5) h	61.46 ± 0.03	6.19 ± 0.76
				779.80 ± 0.05	6.8 ± 0.7
				1111.04 ± 0.10	1.44 ± 0.20
^{198}Hg	8484 ± 3	^{197}Hg	ϵ : (64.14 ± 0.05) h	77.351 ± 0.002	18.7 ± 0.4
				191.36 ± 0.02	0.63 ± 0.02
				268.71 ± 0.03	0.039 ± 0.002
^{204}Hg	7495 ± 2	^{203}Hg	β^- : (46.61 ± 0.02) d	279.197 ± 0.001	81.46 ± 0.13
^{198}Hg	≈ 8962	^{197m}Hg	γ : (23.8 ± 0.1) h	133.08 ± 0.05	33.48 ± 0.26
^{199}Hg	—	^{199m}Hg	γ : (42.6 ± 0.2) min	158.3 ± 0.1	52.3 ± 1.0
				374.1 ± 0.1	13.8 ± 1.1

material which are needed.

IV. EXPERIMENTAL RESULTS

A. $^{196,198,204}\text{Hg}$

Due to the low natural abundance of ^{196}Hg the $^{\text{nat}}\text{Hg}$ targets were activated directly behind the radiator target to use the higher photon intensity at this place of the experimental setup (see Section II). The properties of the activation reactions as well as of the decay of the produced unstable isotopes are summarized in Table II. Figure 3 shows a typical decay spectrum measured after an activation of naturally composed Hg of about 12 hours with $E_{\text{max}} = 9900$ keV.

TABLE III: Results for the normalization σ_0 of Eq. 6 for the reaction $^{196}\text{Hg}(\gamma, n)$.

$E_{\text{max}} / \text{keV}$	E_{γ} / keV	σ_0 / mb
9450	779.80	298 ± 64
	1111.04	266 ± 63
9900	779.80	298 ± 58
	1111.04	267 ± 58
weighted mean $\langle \sigma_0 \rangle$: $(283 \pm 47) \text{ mb}$		

errors and, consequently, the weighted mean $\sigma_0 = (283 \pm 47) \text{ mb}$ has been used to calculate a ground-state reaction rate of $\lambda_{\text{conv}} = (0.42 \pm 0.07) \text{ s}^{-1}$ at $T = 2.5 \times 10^9 \text{ K}$.

2. ^{198}Hg

^{197}Hg is produced in the reaction $^{198}\text{Hg}(\gamma, n)$ if the photon energy exceeds the threshold $S_n = (8484 \pm 3) \text{ keV}$. ^{197}Hg decays by electron capture to ^{197}Au . The most prominent γ lines emitted during this decay have energies of $E_{\gamma} = 191.4$ and 268.7 keV . Both lines stem from the decay of a level at $E(J^{\pi} = 3/2^+) = 268.7 \text{ keV}$ so that the measured yields had to be corrected regarding summing effects.

The direct decay to the ground-state occurs only with rather low probabilities (see Table II) so that the correction of the yield for $E_{\gamma} = 191.4 \text{ keV}$ is in the order of 1% whereas the yield for $E_{\gamma} = 268.7 \text{ keV}$ has to be corrected by about 10%. Another minor correction of both lines are summing effects from x-rays emitted after the electron capture of ^{197}Hg . The resulting yields had to be increased by about 1%.

The three spectra which could be analyzed were sufficient to use the superposition method. The uncertainty of the approximation was in the order of 10%. The resulting reaction rate at $T = 2.5 \times 10^9 \text{ K}$, $\lambda_{\text{super}} = (2.0 \pm 0.3) \text{ s}^{-1}$, is in perfect agreement with the reaction rate that is derived by the conventional method assuming pure s wave decay: $\lambda_{\text{conv}} = (2.0 \pm 0.3) \text{ s}^{-1}$. Thus, the assumed s wave energy dependence of the (γ, n) cross section seems to be correct in the observed energy range from S_n to 9900 keV.

During the activation an isomeric state in ^{197}Hg was populated, too. This state is located at $E = 298.9 \text{ keV}$ and has spin and parity $J^{\pi} = 13/2^+$. It decays with a half-life $T_{1/2} =$

TABLE IV: Results for the normalization σ_0 of Eq. 6 for the reaction $^{198}\text{Hg}(\gamma, n)$.

$E_{\text{max}} / \text{keV}$	E_{γ} / keV	σ_0 / mb
9000	191	294 ± 60
	268	277 ± 59
9450	191	268 ± 46
	268	264 ± 48
9900	191	264 ± 43
	268	291 ± 49
weighted mean $\langle \sigma_0 \rangle$: $(278 \pm 37) \text{ mb}$		

$(23.8 \pm 0.1) \text{ h}$ by electron capture to ^{197}Au with a branching of 8.6%. The state is supposed to be populated in the (γ, n) reaction via an intermediate $J^{\pi} = 9/2^{+}$ state at $E = 478 \text{ keV}$ [19]. Therefore, the effective (γ, n) reaction threshold for isomer population is at about 9 MeV, and we could neither apply the superposition method nor the conventional method.

3. ^{204}Hg

The threshold for the reaction $^{204}\text{Hg}(\gamma, n)$ is located at $S_n = (7495 \pm 2) \text{ keV}$. Only one level in ^{203}Tl is populated in the β^{-} decay of the produced ^{203}Hg nuclei. Because this level decays only to the ground-state by γ ray emission with $E_{\gamma} = 279.2 \text{ keV}$, the yield need not be corrected for summing effects.

The low reaction threshold has the advantage that the decay line could be analyzed in all activation spectra down to $E_{\text{max}} = 8325 \text{ keV}$. This limit is given by the determination of the absolute photon intensity by our calibration standard ^{197}Au ($S_n = 8071 \text{ keV}$).

This limit is a few hundred keV above the threshold of ^{204}Hg , thus, the approximation of the Planck distribution is only possible with large errors of about 20% and yields a reaction rate of $\lambda_{\text{super}} = (57 \pm 9) \text{ s}^{-1}$. To apply the conventional method the energy dependence of the (γ, n) cross section of Eq. 6 is not valid in the observed energy range because the distance to the threshold is too large. One can somehow balance this fact by fitting the exponent to the data and thereby averaging over a broader energy range.

Table V lists the results for the normalization factors σ_0 derived with a fitted ex-

TABLE V: Results for the normalization σ_0 for the reaction $^{204}\text{Hg}(\gamma, n)$. A fitted exponent of $k = 0.85$ was used for the threshold behaviour (see text).

$E_{\text{max}} / \text{keV}$	E_{γ} / keV	$k = 0.85: \sigma_0 / \text{mb}$
8325	279.2	314 ± 54
8550	279.2	277 ± 46
9000	279.2	338 ± 54
9450	279.2	289 ± 46
9900	279.2	307 ± 47
weighted mean $\langle \sigma_0 \rangle$: $(303 \pm 40) \text{ mb}$		

ponent of $k = 0.85$. The reaction rate calculated with the parameters $k = 0.85$ and $\langle \sigma_0 \rangle = (303 \pm 40) \text{ mb}$, $\lambda_{\text{conv}} = (58 \pm 8) \text{ s}^{-1}$, is in excellent agreement with the one derived by the superposition method.

B. ^{204}Pb

Pb is the heaviest element that can be produced in s process nucleosynthesis. The most proton rich stable isotope is ^{204}Pb , a s -only isotope that is shielded against the r process flux by ^{204}Hg . Therefore, ^{204}Pb is besides U and Th one of the heaviest starting points for the p process network calculations on the proton rich side of the valley of stability.

The determination of the (γ, n) reaction rate of ^{204}Pb has been realized with naturally composed target material. Only the reactions $^{204}\text{Pb}(\gamma, n)$ and $^{206}\text{Pb}(\gamma, n)$ produce unstable isotopes and, additionally, no γ rays are emitted during the electron capture decay of ^{205}Pb . Thus, only the γ rays following the electron capture decay of ^{203}Pb are observable in the activation spectra.

The reaction threshold of $^{204}\text{Pb}(\gamma, n)$ is $S_n = (8395 \pm 6) \text{ keV}$. Thus, the decay lines were observable after irradiations with $E_{\text{max}} = 8775, 9000, 9450, \text{ and } 9900 \text{ keV}$. Figure 4 shows a typical spectrum that was measured after an irradiation of about 24 hours with $E_{\text{max}} = 9900 \text{ keV}$.

The half-life of ^{203}Pb is $T_{1/2} = (51.87 \pm 0.01) \text{ h}$. During the electron capture decay two levels at $E(J^\pi = 3/2^+) = 279.2 \text{ keV}$ and $E(J^\pi = 5/2^+) = 680.5 \text{ keV}$ are populated. The

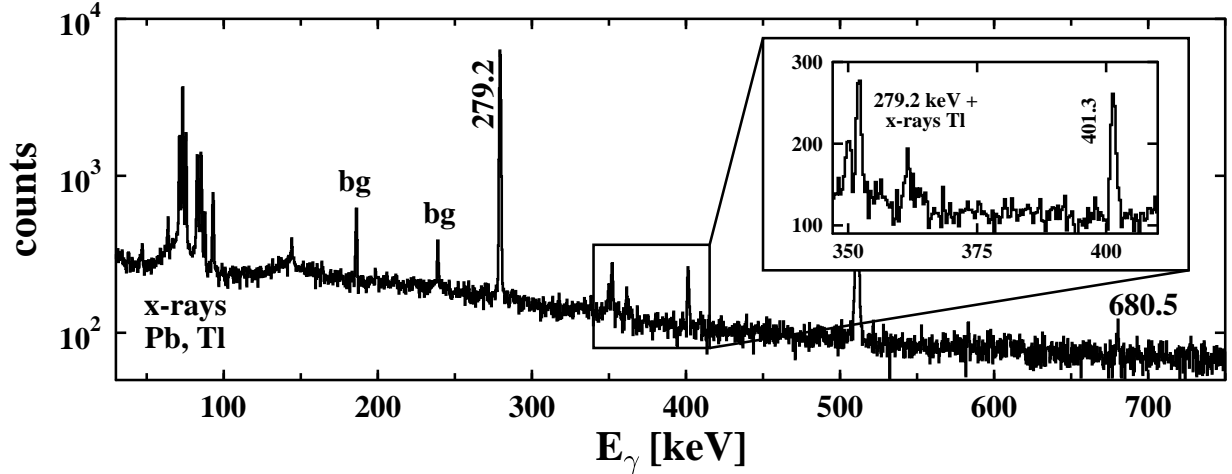


FIG. 4: Typical γ spectrum after photoactivation of naturally composed Pb. The spectrum was measured after an activation of about 24 hours with $E_{\max} = 9900$ keV. The γ lines emitted during the decay of ^{203}Pb are indicated by their energy E_γ while background lines are marked by “bg”. The inset shows the sum of the x-rays of ^{203}Tl and the most prominent γ line with $E_\gamma = 279.2$ keV.

latter decays with a probability of 82% by γ emission to the former one. Therefore, three peaks in the activation spectra at $E_\gamma = 279.2$, 401.3, and 680.5 keV are observable. The line at 680.5 keV is composed by the direct decay of the excited level to the ground-state and the coincident measurement of the two γ rays emitted in a cascade.

The correction for the yield at $E_\gamma = 401.3$ keV was about 7% whereas the yield of $E_\gamma = 279.2$ keV has to be corrected by about 0.2%. A further correction stemming from coincident measurement of the γ rays and the x-rays of the electron capture decay was taken into account with about 6%.

The reaction rate derived at $T = 2.5 \times 10^9$ K by the superposition method is $\lambda_{\text{super}} = (1.87 \pm 0.32) \text{ s}^{-1}$. If the conventional method is used one has to consider that an s wave emission is only possible to an excited level at $E(J^\pi = 1/2^-) = 125.6$ keV in ^{203}Pb . Thus, an effective reaction threshold of $S_n^{\text{eff}} = (8395 + 125.6) \text{ keV}$ has to be used if the energy dependence of the cross section is parameterized as described in Eq. 6.

Table VI summarizes the results for the parameter σ_0 if the effective reaction threshold is used. From the weighted mean a ground-state reaction rate $\lambda_{\text{conv}} = (1.56 \pm 0.25) \text{ s}^{-1}$ at $T = 2.5 \times 10^9$ K is derived which agrees with the result from the superposition method.

TABLE VI: Results for the normalization σ_0 of Eq. 6 for the reaction $^{204}\text{Pb}(\gamma, n)$. An effective threshold of $S_n^{\text{eff}} = 8520.6$ keV was used to calculate σ_0^{eff} .

$E_{\text{max}} / \text{keV}$	E_γ / keV	$\sigma_0^{\text{eff}} / \text{mb}$
8775	279.2	285 ± 73
9000	279.2	414 ± 74
9450	279.2	233 ± 34
	401.3	257 ± 46
9900	279.2	231 ± 31
	401.3	226 ± 34
weighted mean $\langle \sigma_0 \rangle$: (250 ± 40) mb		

V. COMPARISON TO THEORETICAL PREDICTIONS

The aim of our measurements is to test the validity of theoretical predictions of reaction rates at the proton rich side of the valley of stability. Besides the results reported in this paper the reaction rates of platinum isotopes [13] and Au [14] were already determined so that a systematic survey in this region is now complete.

Most of the predictions used for p process network calculations are derived in the Hauser-Feshbach statistical model. The different results rely on the different treatment of the input values e.g. ground-state properties, level densities, optical potentials and γ ray strength functions. Some codes use global parameterizations like NON-SMOKER [19] to become as reliable as possible for unstable and exotic nuclei for which no experimental data is available. Here the masses are taken from experiment or the macroscopic FRDM model with microscopic corrections or the pure microscopic ETFSI-Q approach. The nuclear level densities are derived from a phenomenological Fermi-gas formalism with microscopic corrections and pairing corrections extracted from the above mentioned mass models. The optical potentials and the E1-strength function are derived from global phenomenological descriptions. These approaches using global parameterizations accept the fact that some measured rates are only calculated within an error range of about 25% – 30% [20, 21]. For the NON-SMOKER results shown in table VII experimental masses and the FRDM mass model haven been chosen.

TABLE VII: Comparison of measured and predicted reaction rates at $T = 2.5 \times 10^9$ K. All values are ground-state reaction rates, thus, the thermalization of the target nucleus under p process conditions is not taken into account. Reaction rates predicted with the code NON-SMOKER [19] are indicated by the subscript “NONS” and predictions with the code MOST [22] by “MOST”.

isotope	$\lambda_{\text{exp}}^{\text{super}} / \text{s}^{-1}$	$\lambda_{\text{exp}}^{\text{conv}} / \text{s}^{-1}$	$\lambda_{\text{theo}}^{\text{NONS}} / \text{s}^{-1}$	$\lambda_{\text{theo}}^{\text{MOST}} / \text{s}^{-1}$
^{190}Pt	—	0.4 ± 0.2	0.18	0.29
^{192}Pt	0.5 ± 0.2	0.4 ± 0.1	0.58	0.56
^{198}Pt	87 ± 21	73 ± 17	50	110
^{197}Au	6.2 ± 0.8	5.8 ± 0.8	4.8	5.6
^{196}Hg	—	0.42 ± 0.07	0.32	0.58
^{198}Hg	2.0 ± 0.3	2.0 ± 0.3	1.4	2.1
^{204}Hg	57 ± 9	58 ± 8	73	170
^{204}Pb	1.9 ± 0.3	1.6 ± 0.3	1.5	3.0

Other approaches use experimental data if available and mainly global microscopic or semi-microscopic inputs to reproduce the measured rates very accurately and start their predictions from this basis. An example is the code MOST [22]. Here the masses come from experiment or a microscopic Hartree–Fock–Bogolyubov (HFB–2) model. Nuclear deformations, pairing properties and the single–particle level schemes are derived from the HFB–2 approach. The nuclear level densities stem from a microscopic statistical model including deformation and pairing effects. The nucleon–nucleus optical potential is based on a semi-microscopic Brueckner–Hartree–Fock theory, the alpha–nucleus potential stems from a phenomenological double folding description. Finally the E1–strength function is from a microscopic QRPA calculation. All references can be found in the review article [9].

Our experimental results are compared to the results of both codes in Table VII. It can be seen that the agreement between the experimental data and both predictions is reasonable.

Figure 5 shows the ratio between the theoretical and experimental values. The experimental reaction rates are derived by the superposition method if available. No systematic deviation can be seen in the observed mass region neither for the predictions of the code NON-SMOKER (upper panel) mostly using phenomenological models for the input values nor for the code MOST (lower panel) relying mostly on microscopic models. This can be

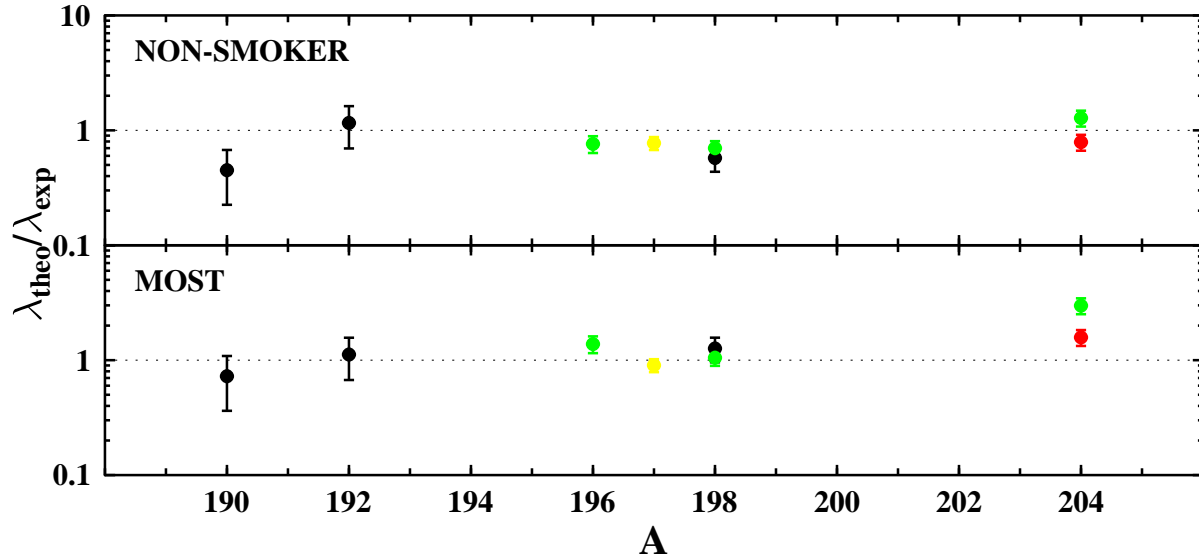


FIG. 5: (Color online) Ratios between theoretically predicted and experimentally derived reaction rates. The upper panel uses the predictions by the code NON-SMOKER [19] whereas in the lower panel the values predicted by the code MOST [22] are used. The black dots correspond to platinum isotopes [13], the yellow one to ^{197}Au [14], the green ones to Hg isotopes, and the red one to ^{204}Pb .

interpreted as a good base for predictions of reaction rates of unstable or exotic nuclei in this mass region. Nevertheless, the deviations for some nuclei range in both cases to factors of up to 2. Thus, further studies seem to be required to improve the nuclear physics input of the codes.

VI. SUMMARY AND OUTLOOK

Theoretical predictions of (γ, n) reaction rates are mandatory as an input for p process network calculations. The validity of the predictions should be tested by comparing the predicted values to experimental ones. Unfortunately, most of the experimental data was measured around the Giant Dipole Resonance, hence, far off the astrophysically relevant energy region.

We have shown that it is possible to determine ground-state reaction rates using the photoactivation technique without any model dependency by a superposition of bremsstrahlung spectra. This method has been used in the mass region $Z \geq 78$ to study the theoretical predictions systematically. No systematic deviation between the experimental rates and those

predicted by the codes NON-SMOKER and MOST have been found.

Due to the high temperatures reached in stellar environments excited levels are populated by thermalization resulting in reaction rates increased by several orders of magnitude. The so-called stellar enhancement factor $\lambda^*/\lambda^{\text{gs}}$ cannot be measured and is fully based on theoretical predictions. The effect is sensitive to level densities and underlying nuclear structure, thus, being a further source of systematic errors.

The mass region $A \approx 100$ is of special interest because this is the border region between the different processes responsible for the production of the p nuclei. A systematic study of the validity of theoretical predictions of (γ, n) and (γ, α) reaction rates would be desirable to improve the understanding of p process nucleosynthesis.

Acknowledgments

We thank the other members of our group especially M. Babilon, W. Bayer, K. Lindenberg, D. Savran, and S. Volz for their support during the beamtime. We also thank P. Mohr and T. Rauscher for valuable discussions. This work was supported by the Deutsche Forschungsgemeinschaft under contract SFB 634.

-
- [1] F. Käppeler, *Prog. Part. Nucl. Phys.* **43**, 419 (1999).
 - [2] G. Wallerstein, I. Iben, P. Parker, A. M. Boesgaard, G. M. Hale, A. E. Champagne, C. A. Barnes, F. Käppeler, V. V. Smith, R. D. Hoffman, et al., *Rev. Mod. Phys.* **69**, 995 (1997).
 - [3] D. L. Lambert, *Astron. Astroph. Rev.* **3**, 201 (1992).
 - [4] F.-K. Thielemann, F. Brachwitz, C. Freiburghaus, E. Kolbe, G. Martinez-Pinedo, T. Rauscher, F. R. W. Hix, M. Liebendörfer, A. Mezzacappa, K.-L. Kratz, et al., *Prog. Part. Nucl. Phys.* **46**, 5 (2001).
 - [5] H. Schatz, A. Aprahamian, V. Barnard, L. Bildsten, A. Cumming, M. Ouellette, T. Rauscher, F.-K. Thielemann, and M. Wiescher, *Phys. Rev. Lett.* **86**, 3471 (2001).
 - [6] S. E. Woosley and W. M. Howard, *Astrophys. J. Suppl.* **36**, 285 (1978).
 - [7] M. Arnould and K. Takahashi, *Rep. Prog. Phys.* **62**, 395 (1999).
 - [8] K. Langanke, *Nucl. Phys.* **A564**, 330c (1999).

- [9] M. Arnould and S. Goriely, *Phys. Rep.* **384**, 1 (2003).
- [10] A. Richter, in *Proc. Fifth European Particle Accelerator Conference* (Institute of Physics Publishing, Bristol, Philadelphia, 1996), p. 110.
- [11] P. Mohr, J. Enders, T. Hartmann, H. Kaiser, D. Schiesser, S. Schmitt, S. Volz, F. Wissel, and A. Zilges, *Nucl. Instr. and Meth. A* **423**, 480 (1999).
- [12] T. Hartmann, J. Enders, P. Mohr, K. Vogt, S. Volz, and A. Zilges, *Phys. Rev. Lett.* **85**, 274; Erratum: *Phys. Rev. Lett.* 86, 4981 (2001) (2000).
- [13] K. Vogt, P. Mohr, M. Babilon, J. Enders, T. Hartmann, C. Hutter, T. Rauscher, S. Volz, and A. Zilges, *Phys. Rev. C* **63**, 055802 (2001).
- [14] K. Vogt, P. Mohr, M. Babilon, W. Bayer, D. Galaviz, T. Hartmann, C. Hutter, T. Rauscher, K. Sonnabend, S. Volz, et al., *Nucl. Phys.* **A707**, 241 (2002).
- [15] S. Müller, to be published (2004).
- [16] P. D. Bièvre and P. Taylor, *Int. J. Mass Spectrom. Ion Proc.* **123**, 149 (1993).
- [17] H. Utsunomiya, H. Akimune, S. Goko, M. Ohta, H. Ueda, T. Yamagata, K. Yamasaki, H. Ohgaki, H. Toyokawa, Y.-W. Lui, et al., *Phys. Rev. C* **67**, 015807 (2003).
- [18] ENSDF, NNDC Online Data Service, ENSDF database, <http://www.nndc.bnl.gov/nndc/ensdf/> (2003).
- [19] T. Rauscher and F.-K. Thielemann, *At. Data Nucl. Data Tables* **75**, 1 (2000).
- [20] T. Rauscher, F.-K. Thielemann, and K.-L. Kratz, *Phys. Rev. C* **56**, 1613 (1997).
- [21] Z. Y. Bao, H. Beer, F. Käppeler, F. Voss, K. Wisshak, and T. Rauscher, *At. Data Nucl. Data Tables* **76**, 70 (2000).
- [22] S. Goriely, in *Nuclei in the Cosmos V*, edited by N. Prantzos and S. Harissopulos (Editions Frontières, 1998), p. 314.